Experimental Study on the Thermoelastic Martensitic Transformation in Shape Memory Alloy Polycrystal Induced by Combined External Forces

PETR SITTNER, YASUHIRO HARA, and MASATAKA TOKUDA

Combined tension and torsion experiments with thin wall specimens of Cu-Al-Zn-Mn polycrystalline shape memory alloy (SMA) were performed at temperature $T = A_f + 25$ K. The general stress-strain behaviors due to the thermoelastic martensitic transformation, induced by a combination of external forces of axial load and torque, were studied. It is shown that the progress of martensitic transformation (MT) at general stress conditions can be well considered as triggered and controlled by the supplied mechanical work (a kind of equivalent stress) in the first approximation. Pseudoelastic strains in proportional as well as nonproportional combined tension-torsion loadings were found fully reversible, provided that uniaxial strains were reversible. The axial strain can be controlled by the change of torque and *vice versa* due to the coupling among tension and torsion under stress, not only in forward transformation, but also in reverse transformation on unloading. The pseudoelastic strains of SMA polycrystal are path dependent but well reproducible along the same stress path. The evolution of macroscopic strain response of SMA polycrystal, subjected to the nonproportional pseudoelastic loading cycles with imposed stress path, was systematically investigated. The results bring qualitatively new information about the progress of the MT in SMA polycrystal, subjected to the general variations of external stress.

I. INTRODUCTION

THE thermally or stress-induced thermoelastic martensitic transformation (MT) in shape memory alloys now seems to be well understood, at least for the most simple single crystal, single interface conditions, for which the vast number of basic experimental and theoretical works have been performed.[1]The progress of the transformation is controlled by the so-called thermoelastic criterion—balance of chemical and mechanical forces driving or opposing the motion of martensite variant interfaces that can be physically well formulated on the atomic level just at the moving martensite variant interfaces.[2] When the external stress or temperature is varied in a proper range, characteristic for each thermoelastic shape memory alloy (SMA), the alloy responds by the nucleation and growth (forward MT) or shrinking (reverse MT) of martensite variant particles. This brings about a macroscopic strain change only if external stress is applied, due to the self-accommodation of crystallographic strains of growing martensite variant particles in stress-free, thermally induced MT. The stresses and strains considered in thermodynamical theory[2] are typically scalars, suitable for experimental single crystal data. The effect of general external stress on the stress-induced, first-order solid state transformations has been discussed in the frame of thermodynamics by Kato and Pak.[3]

On the other hand, the engineering applications of SMA require a simple but reliable estimation of the general macroscopic thermomechanical behaviors of complex polycrystalline SMA for which the single crystal results and models are not directly applicable. For this reason, the transformation behavior of SMA polycrystals is now being widely studied micromechanically on the mesoscopic level. The formulation of the problem through an energetic balance by employing the thermodynamical potential in the form of complementary free energy Ψ associated with the MT in a unit constitutive element is the most powerful and standard current approach.[4,5,6] As an example, Patoor *et al.*[6] introduced the complementary free energy Ψ in the form of Eq. [1], where f represents the volume fraction of transformed martensite phase, $f = \frac{V^M}{V}$, and serves as an internal variable; Σ_{ij} is the external stress; M_{ijkl} is the elastic compliance tensor; T is temperature; B and T_0 are the material constants; and σ_{ij}^{int} is the part of local stress tensor due to the incompatibilities of transformation strain field, $\varepsilon_{ij}^{tr}(r)$.

$$\Psi(\Sigma_{ij}, T, f) = f\frac{1}{V}\Sigma_{ij}\int_v \varepsilon_{ij}^{tr}(r)\,dV - B(T-T_0)f + \frac{1}{2}\Sigma_{ij}M_{ijkl}\Sigma_{kl} + \frac{1}{2V}\int_v \sigma_{ij}^{int}(r)\,\varepsilon_{ij}^{tr}(r)dV \quad [1]$$

While the first two terms represent the part of free energy directly used to convert the parent phase to the martensite structure, the third and fourth terms account for the elastic strain energy and a part of the mechanical energy that has to be stored due to the internal stresses, $\sigma_{ij}^{int}(r)$, created by incompatibilities of transformation strains, $\varepsilon_{ij}^{tr}(r)$, of individual transforming particles. Although a lot of simplifying assumptions and averaging techniques have to be employed in further formulation of the model in order to obtain the simulated general uniform stress-strain-temperature behavior of a constitutive element, the latest simulations provide

PETR SITTNER, Research Associate, formerly with the Faculty of Engineering, Mie University, is with the Institute of Physics, Academy of Sciences of the Czech Republic, Prague, Czech Republic. YASUHIRO HARA, Graduate Student, and MASATAKA TOKUDA, Professor, are with the Faculty of Engineering, Mie University, Tsu, Mie 514, Japan.

Manuscript submitted June 13, 1994.

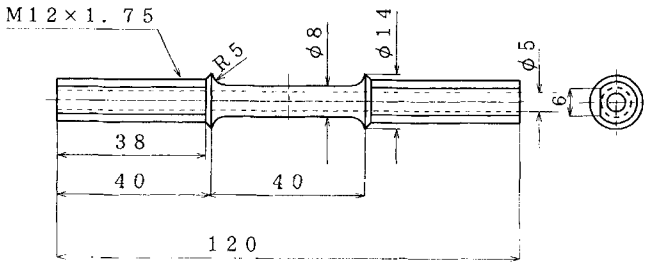

Fig. 1—The shape of the thin wall specimen for combined tension-torsion experiments.

remarkable results for proportional stress conditions.[6] However, the process has a tensorial character in nature, and at present, little is known about the interaction of general stress with thermoelastic martensitic transformation, both experimentally and theoretically.

The evolution of local transformation strains of individual martensite variant particles, $\varepsilon^{tr}_{ij}(r, t)$, during stress- or temperature-induced MT is of prime interest from a material point of view. On the mesoscopic level of SMA polycrystal, we can easily determine only the evolution of the average transformation strain, $E^{tr}_{ij}(t)$, across the volume of transforming polycrystal (Eq. [2]). Here, it will be called the "transformation path."

$$E^{tr}_{ij}(t) = \frac{1}{V}\int_V \varepsilon^{tr}_{ij}(r, t)dV \qquad [2]$$

The constitutive description of thermoelastic MT has to be formulated in terms of uniform stresses, strains, and temperature (Eq. [3]). The measured uniform strain, E_{ij}, is composed of the elastic strain, E^{el}_{ij}, transformation strain, E^{tr}_{ij}, and thermal dilatation strain, E^{th}_{ij}. In spite of the practical rate independency of the experimental stress-strain-temperature behaviors observed, the time has been included to account for the history-dependent deformation behavior of thermoelastic MT in a most simple way. If the external stress, Σ_{ij}, varies in a general nonproportional way during a single thermomechanical cycle, the transformation path defined above need not to be the same in forward and reverse branches of the thermomechanical cycle. This makes a qualitative difference with respect to the standard uniaxial loading tests. What do the transformation paths of thermoelastic MT in SMA polycrystal actually look like at such conditions?

$$E_{ij} = E^{el}_{ij} + E^{tr}_{ij} + E^{th}_{ij} = f(\Sigma_{ij}(t), T(t)) \qquad [3]$$

Also, the ability of shape memory alloys to "memorize" a particular transformation path after a special thermomechanical treatment remains evidently the most exciting feature of these materials. The knowledge of transformation paths of SMA polycrystal under externally enforced nonproportional stress conditions is essential for a proper understanding of the mechanics of shape memory effects exhibited by polycrystals of SMAs. In fact, the growing martensite variant particle should be considered to interact with general nonproportional stress even in uniaxial loading of SMA polycrystal.[4]

This has motivated the experimental study reported in Section II. To simulate general stress conditions, we have chosen a combined tension-torsion loading of thin wall specimens of Cu-10 wt pct Al-5 wt pct Zn-5 wt pct Mn shape memory alloy as a simple and physically well-defined test. When the thin wall tube is subjected to axial load, L, and torque, M, the resulting macroscopic stress state can be characterized as average stress across the volume of the SMA polycrystal, Σ_{ij}. Let us suppose that the thermoelastic MT is induced by the uniform stress Σ_{ij}. It has two nonzero components of axial stress, σ, and torsional shearing stress, τ. Analogically, the average uniform strain, E_{ij}, is given by the axial strain, ε, and torsional shear strain, γ. These components of stress and strain tensors can now be independently controlled or studied. The strain response of SMA polycrystal to the general variation of stress and temperature can be systematically investigated by independent application of external forces of torque and axial load in combined tension and torsion experiments. The experimental data serve as model information about the general stress-strain-temperature thermomechanical behaviors of thermoelastic SMA polycrystal. The results reported here are limited to the transformation pseudoelasticity at constant test temperature.

II. EXPERIMENTAL PROCEDURE

The thin wall specimens for combined tension-torsion experiments were made of Cu-10 wt pct Al-5 wt pct Zn-5 wt pct Mn industrial, polycrystalline SMA produced by Furukawa Co., gage length l = 35 mm (25 mm and 40 mm) and diameters d_{ext} = 8 mm and d_{int} = 5 mm (Figure 1). The specimens were finally heat treated at 873 K for 2 hours and quenched in ice water (grain size, $d \le 120$ μm). Transformation temperatures, found by electric resistivity measurements, are M_s = 239 K, M_f = 223 K, A_s = 248 K, and A_f = 260 K.

A Shimadzu AG-10TS testing machine designed for combined tension-torsion tests with a closed loop servo-control analog system was adapted for simultaneously applied cyclic tension and torsion in force, strain, or mixed control using a PC. A special combined strain extensometer was carefully calibrated to avoid cross effects among tension and torsion strains in the interval of used extensions and angles of rotation. Combined load tests were performed at room temperature T = 285 K (A_f + 25 K) in strain or force control modes. The development of a surface step pattern on an electrolytically polished specimen surface was observed *in situ* by an attached optical microscope.

$$\tau = \frac{16Md_{ext}}{\pi(d^4_{ext} - d^4_{int})}, \qquad \gamma = \frac{d_{ext}\,\theta}{2l} \qquad [4]$$

$$C^S = \frac{\sigma^F}{\tau^F}, \qquad C^E = \frac{\gamma^F}{\varepsilon^F} \qquad [5]$$

$$\tau_{inv} = C^S\tau, \qquad \gamma_{inv} = \frac{\gamma}{C^E} \qquad [6]$$

To determine macroscopic torsional shear stress, τ, and shear strain, γ, from measured torque, M, and torsion angle, θ, the maximum elastic values on the surface of hollow bar specimens were calculated by Eq. [4]. The yield stresses and strains, at which the forward MT starts (σ^F and ε^F in tension and τ^F and γ^F in torsion), were always determined

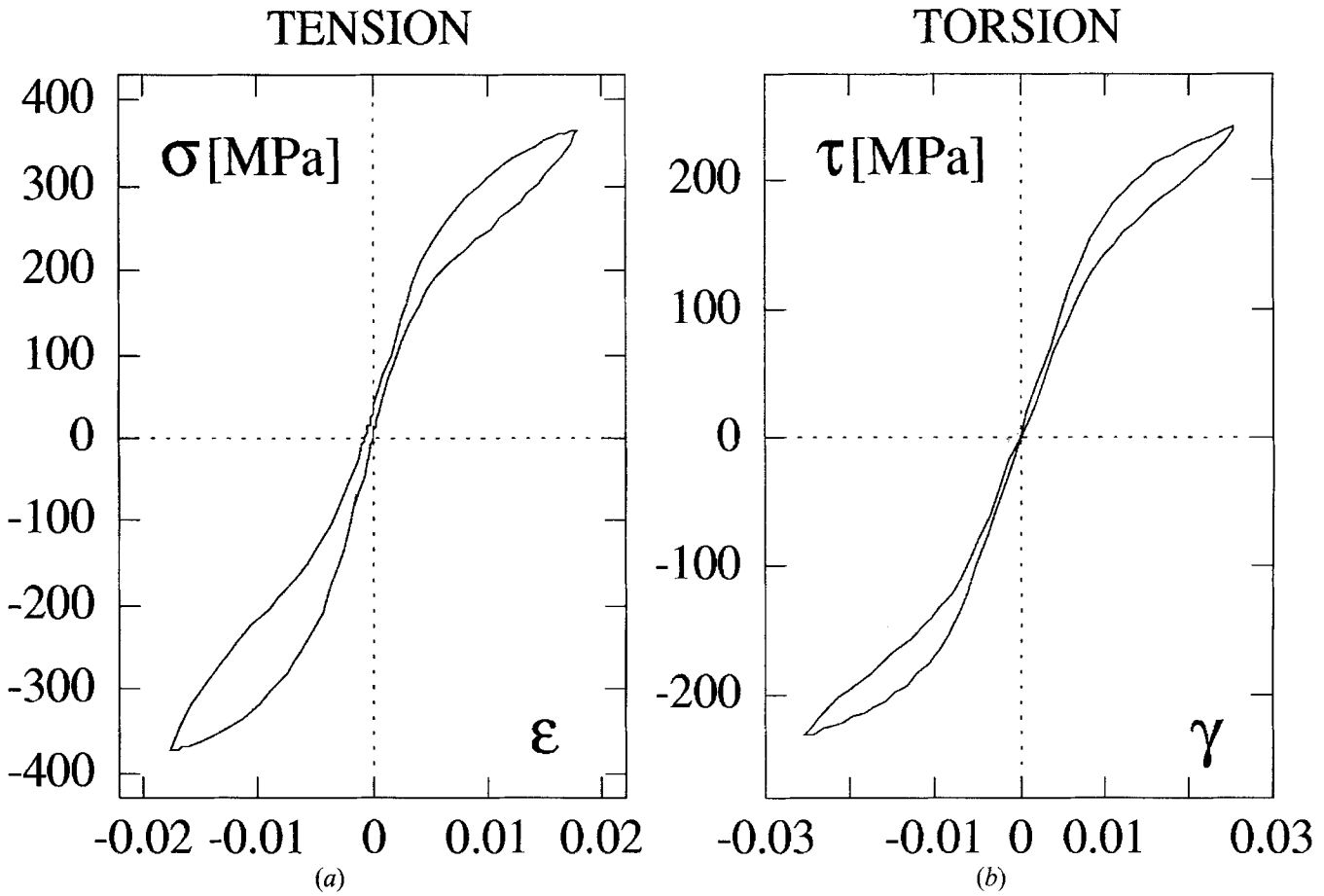

Fig. 2—Uniaxial pseudoelastic stress-strain curves; strain control, T = 285 K: (*a*) symmetrical tension-compression and (*b*) symmetrical torsion+/−.

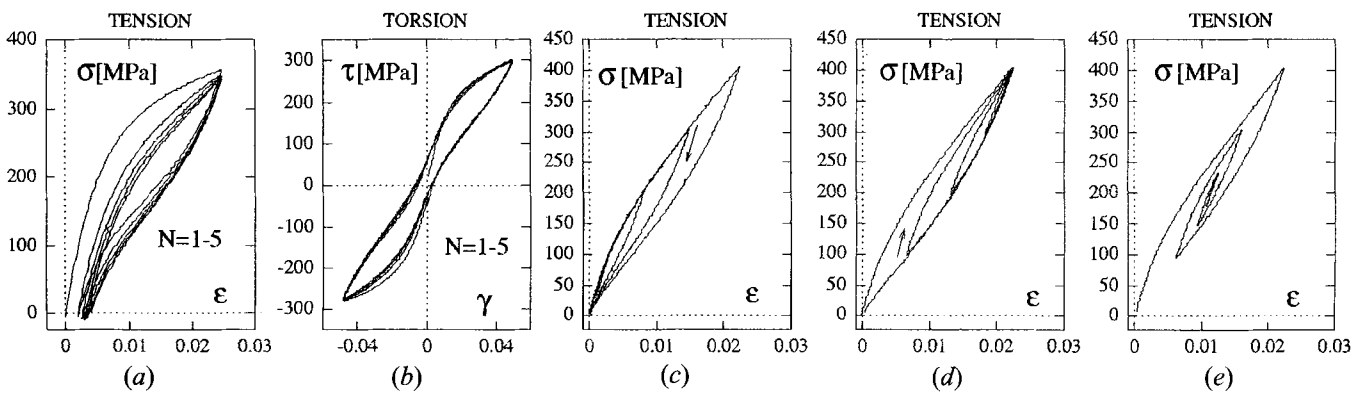

Fig. 3—Uniaxial pseudoelastic stress-strain curves; strain control, T = 285 K: (*a*) tension loading-unloading (five loops), (*b*) symmetrical torsion+/− (five loops), and (*c*) through (*e*) partial pseudoelastic loops in stabilized state in tension.

from the first two pseudoelastic loops on as-quenched specimens. The "0.05 pct proof stress" method was employed to determine the yield points. The empirical coefficients, C^S and C^E, defined by Eq. [5], were calculated for each specimen from the preceding data of the first two loops and used to determine the energetically equivalent values of shear stress, τ_{inv}, and shear strain, γ_{inv}, according to Eq. [6]. The equivalent stresses and strains in simultaneous tension-torsion are calculated by Eq. [7]. Such a technique allows us to determine the energetically equivalent values of uniform stresses and strains in combined tension and torsion without knowing in advance the yield and flow criteria for SMA. It only corresponds to the idea that the amount of elastic energy needed to trigger MT is equal in tension and torsion deformation modes (Section III provides more details). The strain states of the specimen in the combined load test are given by $[\varepsilon, \gamma_{inv}]$ in strain space and their evolution during the pseudoelastic cycle will be called here "strain path," while the sequence of $[\sigma, \tau_{inv}]$ stress states in stress space will be called "stress path". Moreover, the inelastic transformation strains ε^r and γ^r_{inv} are calculated by Eq. [8]. The evolution of transformation strain states, $[\varepsilon^r, \gamma^r_{inv}]$, during the progress of MT represents the transformation path of SMA polycrystal in combined tension-tor-

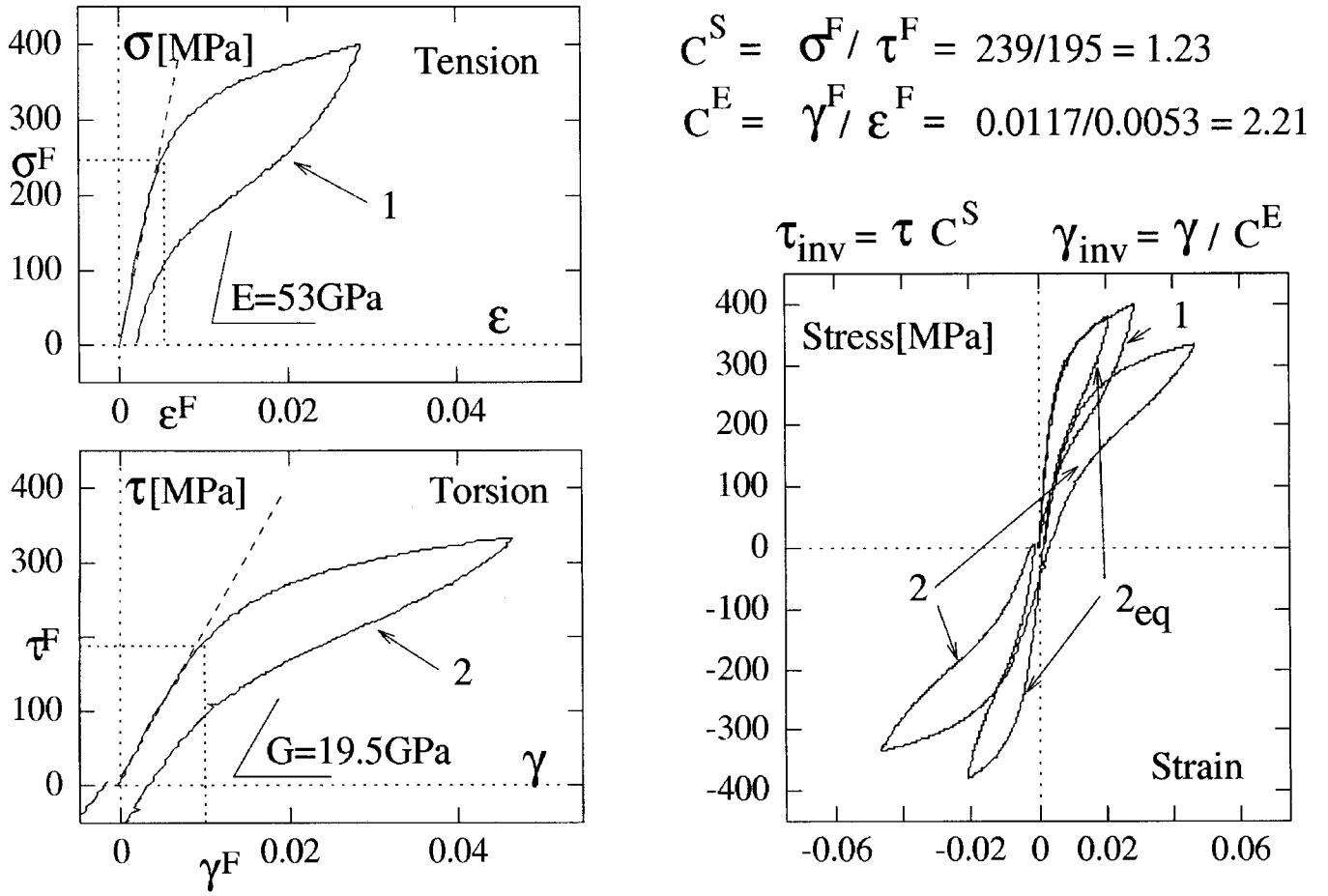

Fig. 4—Uniaxial pseudoelastic stress-strain curves measured on an as-quenched specimen; strain control, T = 285 K: (1) tension and (2) symmetrical torsion+/−. E and G are experimentally determined elastic constants in tension and torsion, respectively; σ^F and ε^F, are critical stress and strain for forward MT induced in tension (τ^F and γ^F in torsion); and 2_{eq} loop is the torsion pseudoelastic loop expressed in equivalent values of shear stress and shear strain.

sion test.

$$\sigma_{eq} = \sqrt{\sigma^2 + (C^S\tau)^2}, \qquad \varepsilon_{eq} = \sqrt{\varepsilon^2 + (\gamma/C^E)^2} \quad [7]$$

$$\varepsilon^{tr} = \varepsilon - \frac{\sigma}{E}, \qquad \gamma^{tr} = \frac{\gamma}{C^E} - \frac{\tau C^S}{E} \quad [8]$$

III. RESULTS AND DISCUSSION

A. *Uniaxial Loading*

Since the basic mechanical characteristics of the pseudoelastic material are described by a standard uniaxial loading-unloading test, the pseudoelastic curves recorded in symmetrical tension-compression (Figure 2(a)) and symmetrical torsion +/− (torsion right-torsion left) (Figure 2(b)) tests are shown here to introduce the SMA material used. The specimens used for compression tests are of slightly different shape with shorter gage length (l = 25 mm, d_{ext} = 8 mm, and d_{int} = 5 mm) and smoother transition to the specimen head. The steps corresponding to martensite variant particles, activated in surface grains, were observed *in situ* on the specimen surface during the first two symmetrical tests as appeared, grew, and disappeared on unloading. The growth or shrinking of a martensite variant particle proceeded *via* sudden bursts along the habit plane but continuously in the direction perpendicular to the habit plane. The particles were distributed highly inhomogeneously on the surface area observed in deformed state. The steps observed in the same arbitrarily chosen place in tension, compression, torsion+, and torsion− deformation modes were mostly of different orientations. This happens due to the well-known asymmetry of the interaction of MT with the +/− orientation of the shear stress.[1,8] The experimental data of symmetrical pseudoelastic loops, however, suggest a good isotropy of the stress-strain behaviors on the mesolevel of Cu-Al-Zn-Mn SMA polycrystal. While the first torsion +/− pseudoelastic loops are always perfectly symmetrical, the tension-compression mechanical behaviors regularly exhibit slight asymmetries (for example, in the width of hysteretic loops). However, the martensite start stresses, σ^F, and the slopes of stress-strain loops in the transformation flow region are practically identical in tension and compression if the correction for true stress is made. Such tension-compression deformation behavior is in sharp disagreement with experimental data, obtained on some other SMA alloys as Cu-Zn-Al or Ni-Ti, where large dissymmetry among tension and compression deformation behaviors has been recently reported (discussion and references in Reference 9).

It is a common experience with polycrystalline SMA that the shape of pseudoelastic stress-strain loops changes essentially in several introductory loops and then remains almost unchanged for a large number of cycles (Figures 3(a)

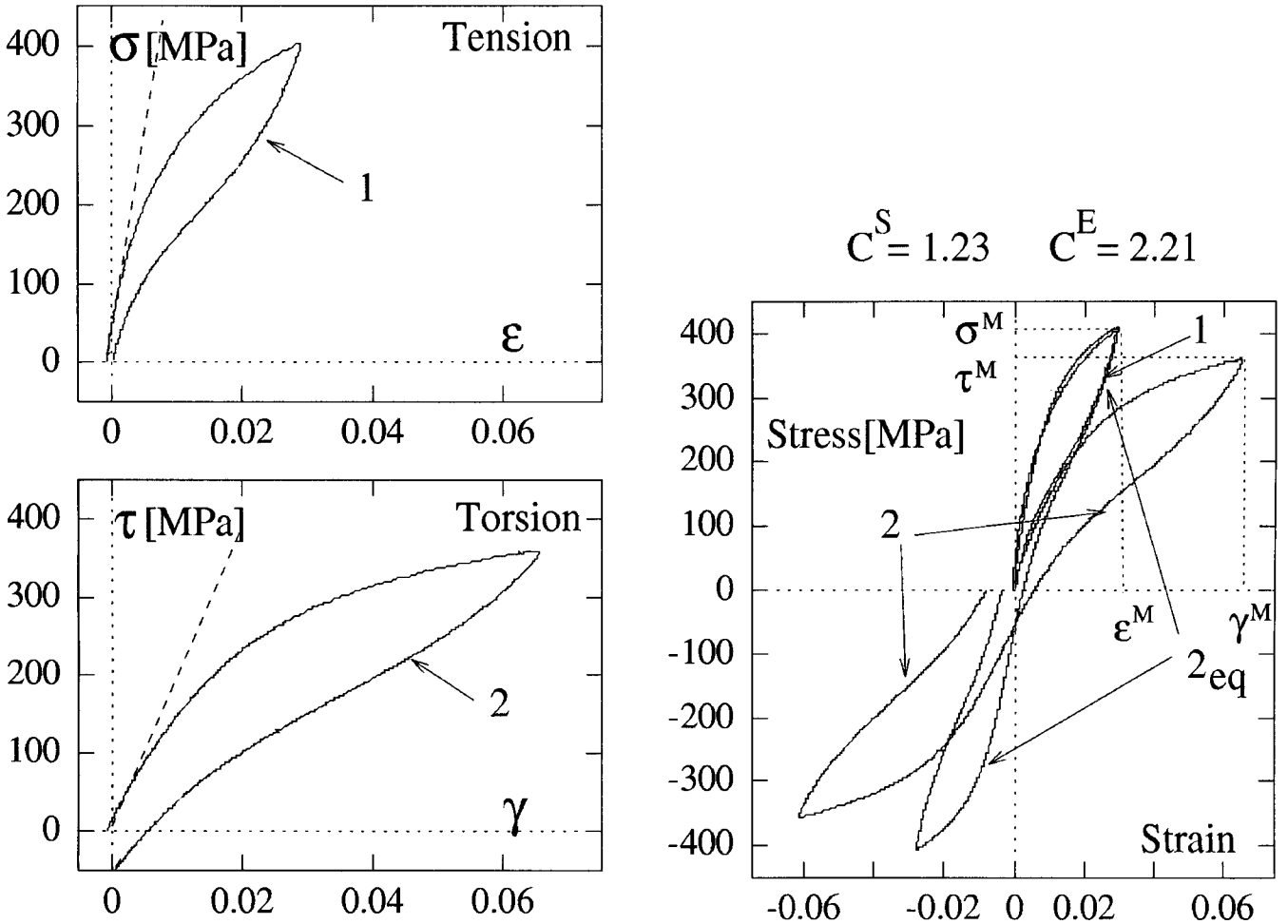

Fig. 5—Uniaxial pseudoelastic stress-strain curves measured on a specimen in mechanically stable state; strain control, T = 285 K: (1) tension (7th loop) and (2) symmetrical torsion+/− (11th loop). ε^M and γ^M are maximum imposed strain and shear strain, and σ^M and τ^M are the maximum recorded stress and shear stress, respectively; 2_{eq} loop is the torsion pseudoelastic loop expressed in equivalent values of shear stress and shear strain.

and (b)). In order to bring the specimen into a relatively stable mechanical state, together at least ten introductory loops in all deformation modes used were necessary. When the introductory loops were performed along the same (similar) strain path, an essential strain anisotropy was introduced into the microstructure of the specimen. Consequently, a measurable nonproportionality among stress and strain paths was observed in subsequent deformation tests, as reported in Reference 10. After such an initial cycling, the stress-strain curves become approximately stabilized. The stress-induced MT becomes mechanically reversible, nevertheless, due to the dissipative nature of thermoelastic MT; the stress-strain behavior still displays the well-known, complicated hysteretic character. Examples of axial loading-unloading pseudoelastic curves in stabilized state, including various partial loops, are shown in Figures 3(c) through (d). The following should be noted.

(1) Martensitic transformation is not completed at the maximum stress even in the largest pseudoelastic loop.
(2) The width of hysteresis of the partial loop depends essentially on the minimum-maximum stress difference.
(3) All partial loops are always perfectly closed (on return, they pass exactly through the same stress-strain state, where they have been started).
(4) All the stress-strain states, enclosed by the experimental hysteretic loop of maximum area, can be repeatably reached by properly chosen deformation paths.

The partial loops were included here, since we believe that the key to the mechanical description of stress-induced MT lies in the proper understanding of the preceding hysteretic behaviors.[7]

Due to the changes of the shape of the pseudoelastic loop with the number of cycles, only the first tests in each deformation mode on as-quenched specimens bring meaningful information about the critical stresses σ^F and τ^F to induce forward MT. Two such pseudoelastic loops, performed on a single specimen, are shown in Figure 4. The shear stress, τ, and shear strain, γ, represent the maximum values on the surface of still a relatively thick wall tube and are not fully appropriate for the description of the uniform strain and stress states of the transforming specimen. Due to this uncertainty and, at the same time, due to the need for definition of equivalent stress but lacking the knowledge about yield and flow criteria for SMA polycrystal, we introduced directly the energetically equivalent values of shear stress, τ_{inv}, and shear strain, γ_{inv}, in torsion. If the torsion pseudoelastic curve is drawn in $\tau_{inv}$and γ_{inv} coordinates (2_{eq} loop), the phenomenologically evaluated density of elastic energy, necessary to trigger MT, is by

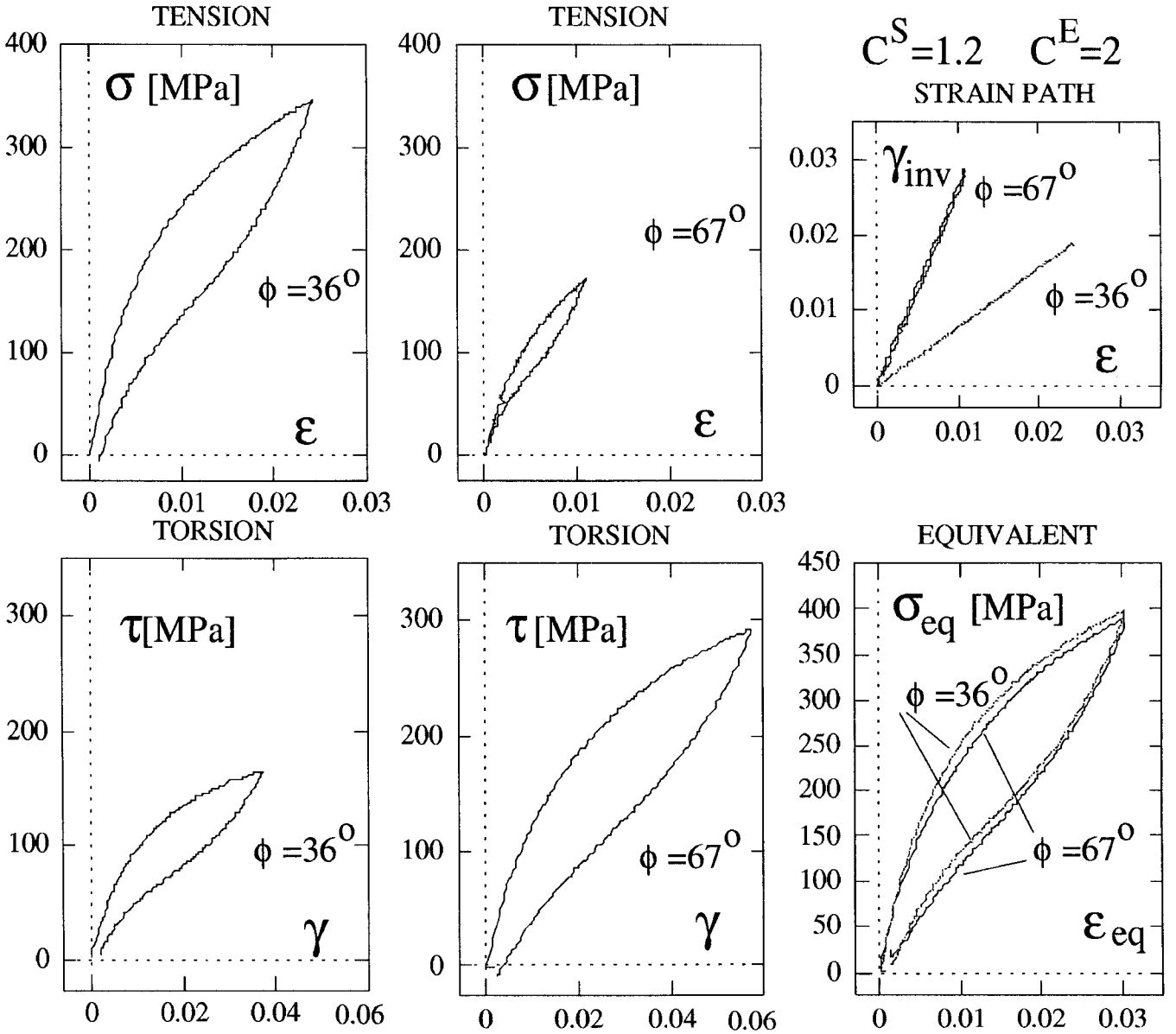

Fig. 6—Two combined tension-torsion proportional tests; strain control, T = 285 K; the imposed strain paths are characterized by the maximum equivalent strains, ε_{eq}^{M} = 0.03, and an orientation angle in strain space, ϕ = arctg ($\gamma_{inv}^{M}/\varepsilon^{M}$), ϕ = 36 or 67 deg).

definition equal in tension and torsion tests. However, as we can see in Figure 4, not only the critical stresses and strains coincide, but also all of the forward branches of both pseudoelastic loops recorded in tension and torsion automatically fit one another as a result. Since we newer knew the exact values of C^S and C^E coefficients in advance, we could not know at which shear strain to reverse the run of the torsion test. The maximum stresses of first tensile and first torsion loops are, therefore, different. The character of $\sigma - \varepsilon$ and $\tau - \gamma$ pseudoelastic loops changes essentially in subsequent pseudoelastic cycles (Figures 3(a) and (b)); nevertheless, the once determined coefficients for calculation of equivalent stresses and strains result in a very good fit of all of the pseudoelastic loops in stabilized state. (In Figure 5, the 7th tensile and 11th symmetrical torsion loops are brought together, and the maximum shear strain $\gamma^M = C^E\varepsilon^M$ is applied in the torsion test.) The scheme, of course, can be used for fully reversible strains only. We will further use τ_{inv} and γ_{inv} for the description of shear stress and shear strain instead of τ and γ, since the main goal of this study is the investigation of transformation paths in nonproportional loadings and the scale on the y-axes of stress and strain spaces is of lesser importance than the shape of transformation pathways itself.

B. *Proportional Combined Loading*

Pseudoelastic loading-unloading behavior under a constant ratio of axial and torsional strain increments (proportional loadings) was examined on a specimen already brought into the mechanically stable state by performing introductory cycles in tension and torsion +/−. A set of strain control experiments [$(\Delta\gamma/\Delta\varepsilon)$ = const.] with prescribed linear strain paths was performed, and the stress response was measured. The maximum equivalent strains in each test were ε_{eq}^{M} = 0.03. The tension and torsion strains were applied simultaneously, and as a result, the transformation paths in forward and reverse MT were identical in this case.

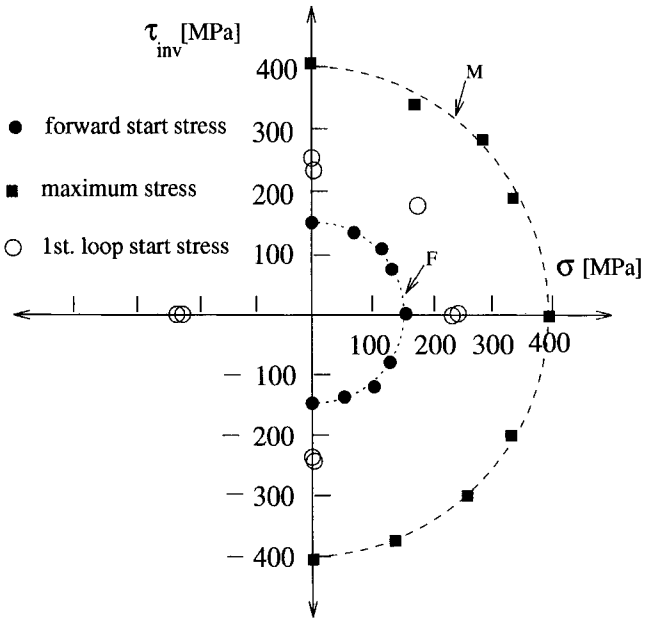

Fig. 7—The forward MT start stress states (F) and maximum stress states (M) in proportional combined tension-torsion tests; T = 285 K; mechanically stable loops; ε_{eq}^{M} = 0.03; forward MT start stress states in the first tests (as-quenched specimens) are shown by ○.

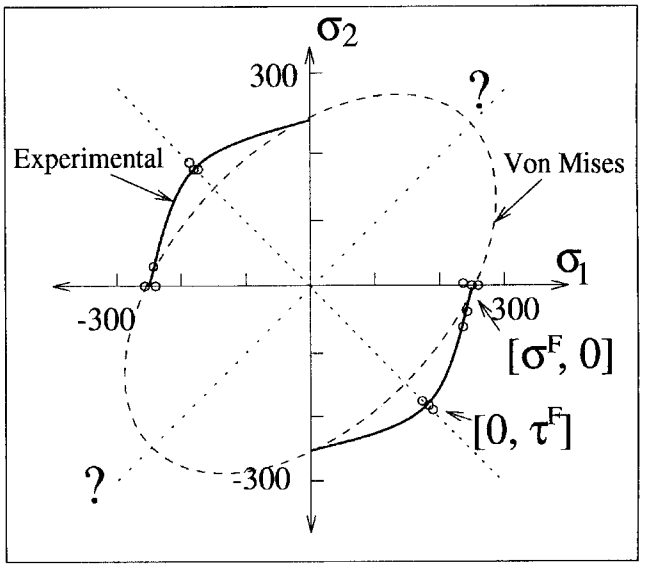

Fig. 8—The experimental transformation yield surface in principal stress space, recalculated from [σ^F, τ^F] forward MT start stress states determined from the first two pseudoelastic loops on different specimens; T = 285 K.

The stress-strain behavior studied in combined load test is fully characterized as a time sequence of [σ, τ] stress and [ε, γ] strain states. However, the invariant values of shear stress and shear strain for torsion are used to present the stress and strain paths in corresponding stress and strain vector spaces. The length of the strain (stress) vector in such coordinates is the equivalent strain, ε_{eq} (equivalent stress, σ_{eq}). The pseudoelastic loops, recorded separately by tension and torsion controllers, are always drawn in $\sigma - \varepsilon$ and $\tau - \gamma$ coordinates (Figure 6) in order to present the undistorted data as well. When the critical stress states [σ^F, τ_{inv}^F] for forward MT are evaluated from such curves and drawn in $\sigma - \tau_{inv}$ stress space (Figure 7), they lie quite well on a half-circle with the diameter σ_{eq} = 150 MPa. Compression experiments could not have been performed on the longer (l = 35 mm) specimen and are not included. The part of such a "transformation yield surface" in the form of a half-circle does not automatically imply that the material obeys the von Mises yield criterion because of the definition of τ_{inv} in torsion (the $C^S \neq \sqrt{3}$). Not only the transformation start stress states but also the recorded maximum stress states [σ^M, τ_{inv}^M] reached in each test lie quite well on the half-circle in the stress space. Finally, when we draw the equivalent stress–equivalent strain, $\sigma_{eq} - \varepsilon_{eq}$, curves, they fit each other similarly to the special cases of pure tension and pure torsion tests shown. We do not know from these experiments if the mechanical energy needed to trigger MT is really equal in tension and torsion deformation modes. We may conclude, however, that the amount of the supplied mechanical work in combined tension-torsion loadings, characterized by the value of equivalent stress, controls very well both the start and the overall progress of MT.

The application of tension, torsion, and compression loadings to SMA material provides, nevertheless, a unique opportunity to determine part of the transformation yield surface. The problem is the change of the shape of the pseudoelastic loops with the number of cycles performed that limits us to the first two pseudoelastic loops on each specimen. Also we take the shear stress, τ, as representative for not really thin wall specimens. The principal stresses σ_1 and σ_2, calculated from the transformation start stress states [σ^F, τ^F] recorded in the first two pseudoelastic loops on each specimen in various tests (tension, compression, torsion +/−, and simultaneous tension-torsion), are drawn in principal stress space. The part of the transformation yield surface constructed in this way is shown in Figure 8, where the symmetry along the biaxial stress axis is reasonably supposed. One can see that the determined branches of experimental transformation yield surface slightly differ from the theoretical von Mises ellipse drawn through the [σ^F, 0] stress state. Anyway, if the SMA material obeys the von Mises yield criterion (if the MT is triggered by the critical elastic energy of distortion) and the τ and σ well characterize the uniform stress state, the experimentally determined coefficient C^S should approach the theoretical $\alpha = \sqrt{3}$ value. One must be very careful to use only the data of first symmetrical loops on as-quenched specimens to determine the transformation start stresses. If, for example, ten pseudoelastic loops are performed in tension only (as in Figure 3(a)) and the 11th loop is a symmetric tension-compression one, the absolute value of σ^F in compression, evaluated by the "0.05 pct proof stress" method by using the original elastic constant E, could be 100 pct higher than σ^F of the tension part of the symmetrical loop. Also, the slopes of stress-strain loops in the transformation regions in tension and compression would be very different.

C. *Nonproportional Combined Loading*

When the SMA polycrystal is subjected to the nonproportional loadings (for example, torsion at applied axial force), the uniform stress changes in a nonproportional way. The existing martensite variant particles, already induced

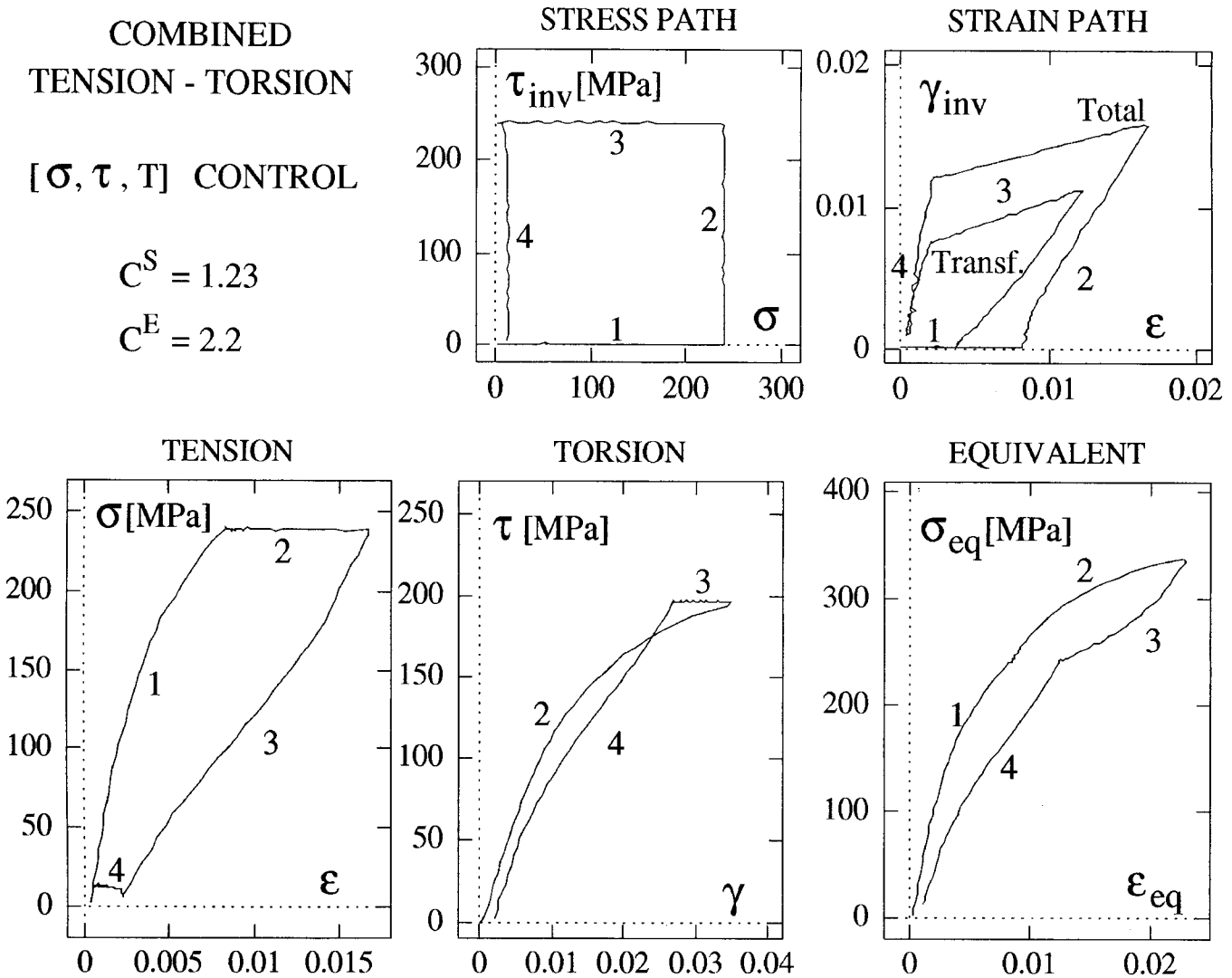

Fig. 9—Nonproportional combined load test; stress control, T = 285 K; fifth loop; the subsequent stages of the test are numbered 1 through 4; both the strain path (total) and transformation path (transf.) are drawn in strain space.

by axial stress in the previous deformation history, need not be the most favored ones by the external stress anymore, stop to grow, interact with other newly nucleated particles, or even shrink back to the parent phase. What is the macroscopic stress-strain behavior of SMA polycrystal with misorientated crystal grains under such loading conditions? This has been systematically studied using nonproportional combined load tests.

The stress path is imposed in a stress control test (Figure 9), and the response of the specimen is illustrated by the separate pseudoelastic loops $\sigma - \varepsilon$ and $\tau - \gamma$, strain path and transformation path in strain space, and equivalent stress-strain, $\sigma_{eq} - \varepsilon_{eq}$, loop. The first important result is that the pseudoelastic strains in a nonproportional loop are again completely reversible. The shape of $\sigma - \varepsilon$ and $\tau - \gamma$ pseudoelastic loops becomes rather exotic, since they separately contain only part of the information about the stress-strain constitutive behavior, expressed by Eq. [3]. On the other hand, the equivalent stress-strain $\sigma_{eq} - \varepsilon_{eq}$ curve fits the shape of the uniaxial loading-unloading pseudoelastic loop. The $\sigma_{eq} - \varepsilon_{eq}$ loop characterizes the mechanical energy stored in each stage of the nonproportional test (compare Figures 4 and 9, with different specimens and similar maximum equivalent strains). If we consider the area enclosed by the $\sigma_{eq} - \varepsilon_{eq}$ loop (or better the sum of areas enclosed by $\sigma - \varepsilon$ and $\tau_{inv} - \gamma_{inv}$ separate loops) as a measure of the total dissipated energy in a nonproportional loop, we observe that the energy dissipation in the nonproportional test is not any larger than in the proportional one. This justifies the usage of Eqs. [6] and [7] even for nonproportional tests. The shape of strain paths documents a coupling among tension and torsion under stress not only in forward MT (as typically observed in metal plasticity and described in plasticity theory by the yield criterion and the flow rule for loading) but also on unloading due to the reverse MT.

The transformation path can be better controlled in a strain control test, as shown on Figure 10. The evolution of external stress as a system response, however, exhibits a very complicated behavior (the opposite torque force has to be applied during reverse branch of the strain control loop). Nevertheless, the equivalent stress-strain, $\sigma_{eq} - \varepsilon_{eq}$, loop still corresponds relatively well to the tensile pseudoelastic loop. Since it is the stress that controls the progress of thermoelastic MT, we prefer the stress control experiments with well-defined stress paths imposed, in or-

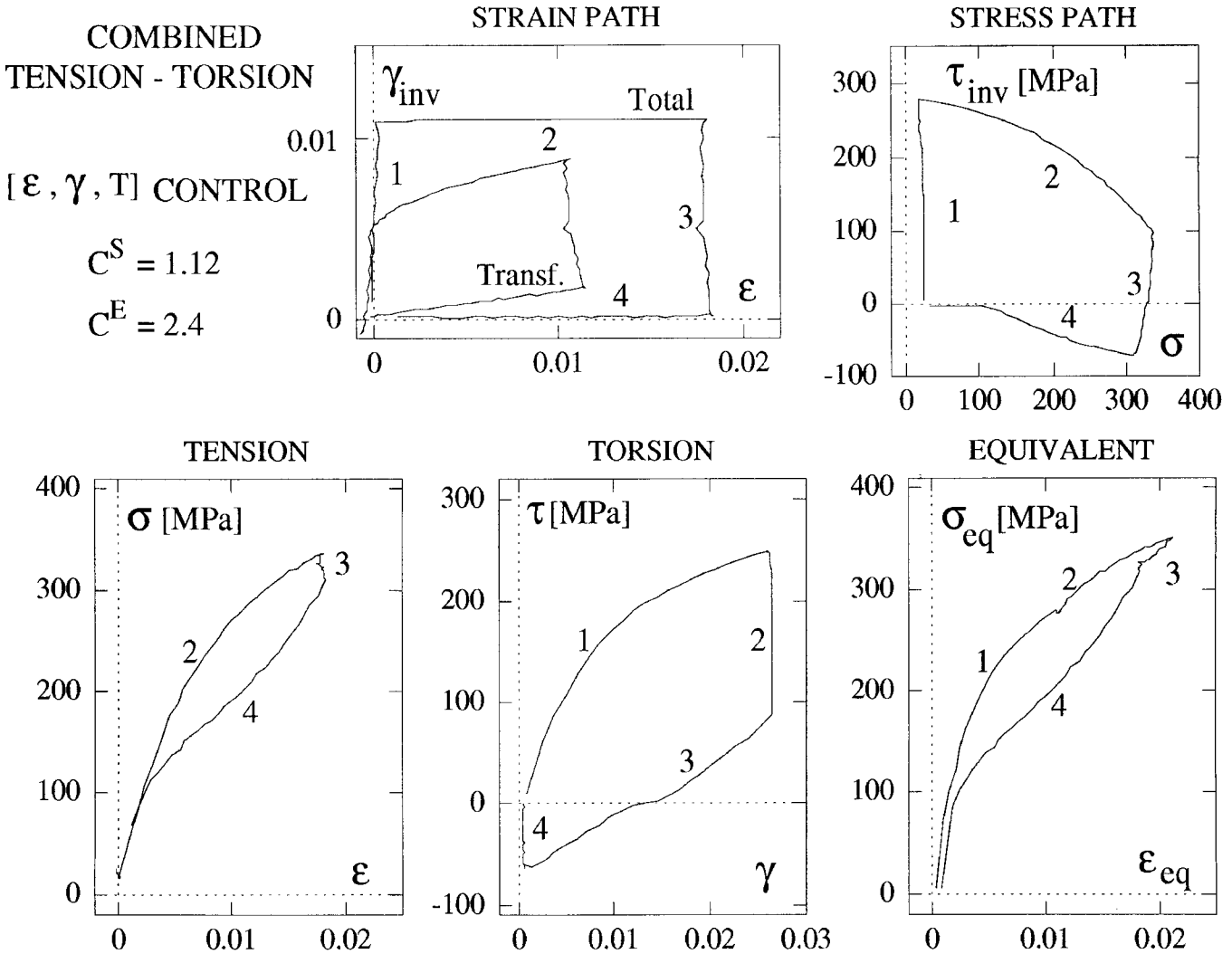

Fig. 10—Nonproportional combined load test; strain control, T = 285 K; third loop; the subsequent stages of the test are numbered 1 through 4; both the strain path (total) and transformation path (transf.) are drawn in strain space.

der to get one continuous forward loading [$(dG_{eq}/dt) > 0$] up to the maximum stress state, followed by one continuous unloading [$(dG_{eq}/dt) < 0$] back to the original stress state [0,0]. The stress control mode is also physically acceptable due to the practical rate independency of stress-strain behaviors and due to the large slope of experimental stress-strain curves in the mechanically stable state (Figures 3(c) through (e)).

It thus has been shown that the deformation behavior of pseudoelastic SMA polycrystal under nonproportional stress conditions can be well characterized by the supplied mechanical work (equivalent stress). The equivalent stress-strain curve, $\sigma_{eq} - \varepsilon_{eq}$, characterizes the progress of MT in SMA polycrystal at general nonproportional stress conditions in the similar level of approximation as the tensile $\sigma - \varepsilon$ curve for uniaxial stresses and strains. The evolution of the average transformation strain in a nonproportional pseudoelastic cycle is, however, path dependent and reflects the strong shear stress sensitivity of MT.

D. *Transformation Pathways in Combined Loading*

The strain response of SMA polycrystal to the prescribed evolution of stress states deserves special attention and will be discussed in this section. As we have already seen, the response of the as-quenched specimen in a proportional loading test is indeed proportional to the imposed linear strain (stress) path. This proportionality is lost if the specimen has been mechanically loaded repeatedly along the same (similar) strain path in previous deformation history.[10]

Interesting mechanical features of the general stress-induced MT appear in nonproportional tests in the form of the recorded strain (stress) response to the simple imposed stress (strain) paths. We performed a systematic investigation of transformation paths of SMA polycrystal using simple stress paths imposed in stress control experiments (Figure 11) in order to understand the path dependency of general stress pseudoelastic behaviors. Some results are summarized in Figures 12(f) through (j). The stress paths recorded in strain control experiments (Figures 12(a) through (e)) were included just to compare the response of SMA polycrystal in both control modes. Other experimental data can be found in References 11 through 13.

Let us compare the strain paths recorded in two nonproportional tests along different stress paths to a single maximum stress state $A = [\sigma^M, \tau^M_{inv}] = [300,190]$. One can see that pseudoelastic strains are completely reversible, and practically the same maximum equivalent strains, $\varepsilon^M_{eq} \approx 2.5$ pct

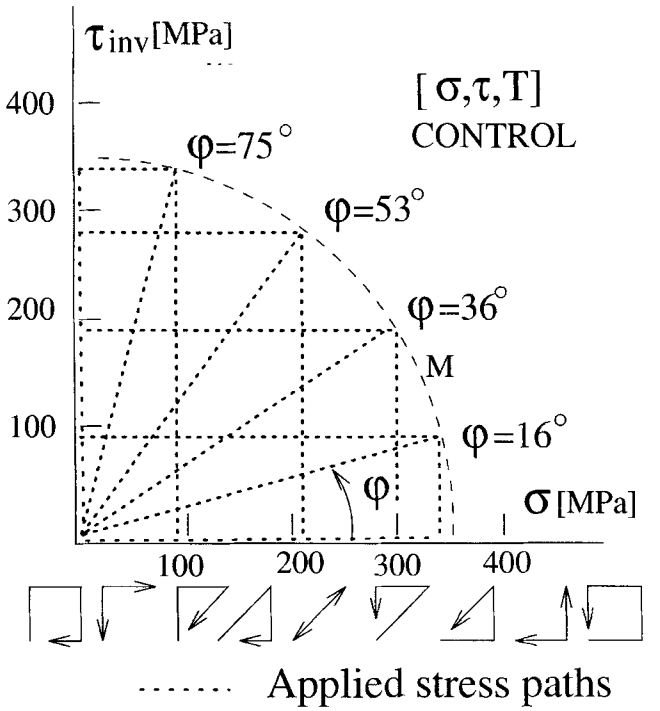

Fig. 11—The stress paths imposed in nonproportional tests; T = 285 K; maximum stress states $[\sigma^M, \tau^M_{inv}]$ are defined by the σ_{eq} = 350 MPa and orientation angle in stress space φ = arctg (τ^M/σ^M); the shapes of stress paths are suggested schematically.

(the distance from the origin [0,0] in strain space), have been reached regardless of the applied stress path. Nevertheless, the maximum strain states reached are different if different stress paths toward the A point are imposed (Figures 12(f) through (j)). The scatter among B, $B1$, and $B2$ in strain space for the simple stress paths used, however, is smaller than 0.3 pct in spite of the large inelastic strain corresponding to the maximum equivalent strain.

We thus find that the average transformation strains of SMA polycrystal depend on the shape of the already passed transformation path (elastic strains are path independent and given solely by the external stress according to Hook's law). The strain of a uniaxially deformed specimen also depends on the previous deformation history (various strains correspond to a single stress due to the energy dissipation and mechanical hysteresis, refer to partial loops in Figure 3(e)). The difference is that in combined loading, we deal with energy dissipation along the forward transformation branch only. Indeed, the scatter among maximum strain states, corresponding to a single maximum stress state, approached along various stress paths is just another consequence of the energy dissipation during the process of the stress-induced MT. The energy dissipation takes place along different transformation paths, and the obtained maximum strain states, B, $B1$, and $B2$, are different from each other, while the same strain state is reached with good reproducibility along the same stress path. The scatter among maximum strain states generally increases with the σ^M_{eq}, since the amount of dissipated external work is larger in this case. Also, when both forward and reverse MT have already taken place along one of the strain paths, the scatter among strain states corresponding to a single stress state can be significantly larger (refer to the strain states C^F and C^R corresponding to a stress state C reached along various stress paths in Figures 12(g) through (j)). In the limit of SMA materials with very small width of hysteresis loop, the pseudoelastic behaviors would still be shear sensitive but almost path independent ($B = B1 = B2$) in our opinion. The shape of the strain paths in stress control nonproportional tests (as in Figure 12(j)) would be the same whether the test proceeds clockwise or counterclockwise. On the other hand, if the energy dissipated is so large that the transformation strains become irreversible, Eqs. [6] and [7] do not describe well the equivalent strain even in the forward branch of the pseudoelastic cycle.

Finally, we were interested in transformation flow of SMA polycrystal under combined forces. Specially designed experiments were performed to study systematically the strain response of a partially transformed SMA polycrystal to the general stress changes. The results are shown on Figure 13. The specimen was deformed ten times; it was deformed first in torsion up to the stress state $[\sigma,\tau_{inv}]$ = [0,250], and then loading was continued further along ten various stress paths a through j up to the maximum equivalent stress, σ^M_{eq} = 300 MPa (Figure 13(a)). Only forward branches of stress paths of the tests are analyzed. The σ^M_{eq} is a little smaller than 300 MPa in tests g and i due to control errors. The recorded evolution of macroscopic strains (strain paths, Figure 13(b)) and average transformation strains (transformation paths, Figure 13(c)) provides systematic information about the behavior of stress-induced martensite subjected to the various types of general stress changes.

At first, it should be noted that regardless of the shape of the applied stress paths a through j, the maximum strain states, $[\varepsilon^M, \gamma^M_{inv}]$, corresponding to the maximum equivalent stress σ_{eq} = 300 MPa are again located near the half-circle in strain space in accord with the previous results. This is not necessarily true for transformation strains, particularly the maximum transformation strains corresponding to the c through f stress paths. In tests a through c, the transformation strains develop partially further in torsion+ after the change of stress path direction, as would be largely expected, since the mechanical work continues to be supplied, $(d\sigma_{eq}/dt) > 0$. The reverse transformation clearly proceeds ($\Delta\ \gamma^r_{inv} < 0$ and $\Delta\varepsilon^r = 0$) after the change of stress path direction in tests g through j, but it is completed only in cases i and j (?h). What happens along the stress paths d through h? The reverse MT does start on reloading when σ_{eq} decreases in d through f cases but temporarily stops when the minimum of equivalent stress is passed and the mechanical work again becomes supplied. The forward MT starts again in the new direction, now driven mainly by the prevailing axial stress. The transformation paths g and h are the most interesting ones. There is a large transition region between the reverse MT and forward MT on reloading, and the torsion component of transformation strain decreases even if the mechanical work is being supplied. The strain responses from whole nonproportional pseudoelastic loops e, f, and h are compared with the evolution of σ_{eq} (supplied mechanical work) in Figure 14. Do the martensite variant particles nucleated in the beginning torsion+ branch of the applied stress path shrink when the mechanical work is being supplied on reloading along stress paths g and h? Does the reorientation of stress-induced martensite particles take

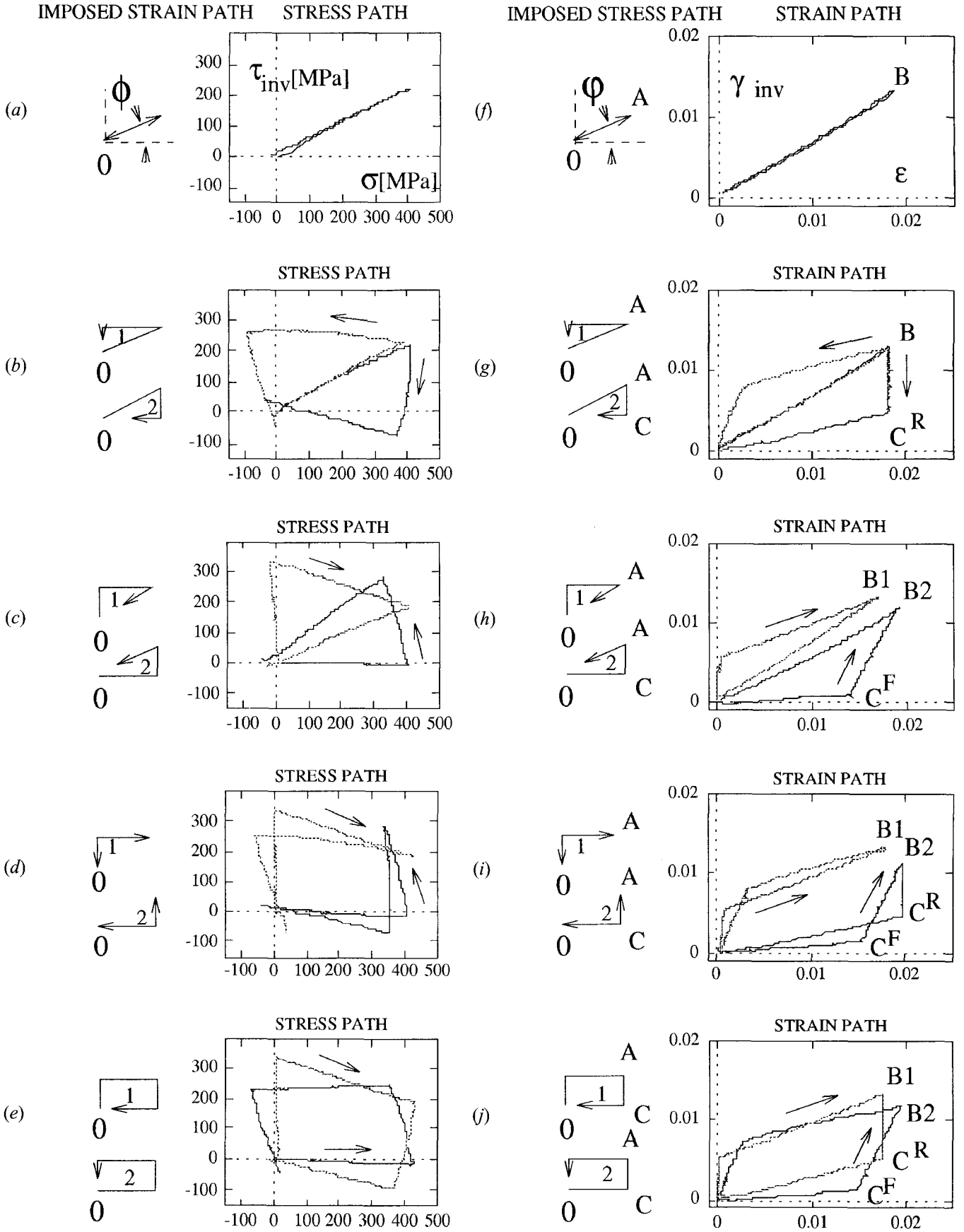

Fig. 12—Stress path responses from strain control tests (*a*) through (*e*) ($\varepsilon_{eq}^{M} = 0.03$, $\phi = 36$ deg) compared with strain path responses from stress control tests (*f*) through (*j*) ($\sigma_{eq}^{M} = 350$ MPa, $\varphi = 36$ deg); $T = 285$ K; the shapes of imposed paths are suggested schematically.

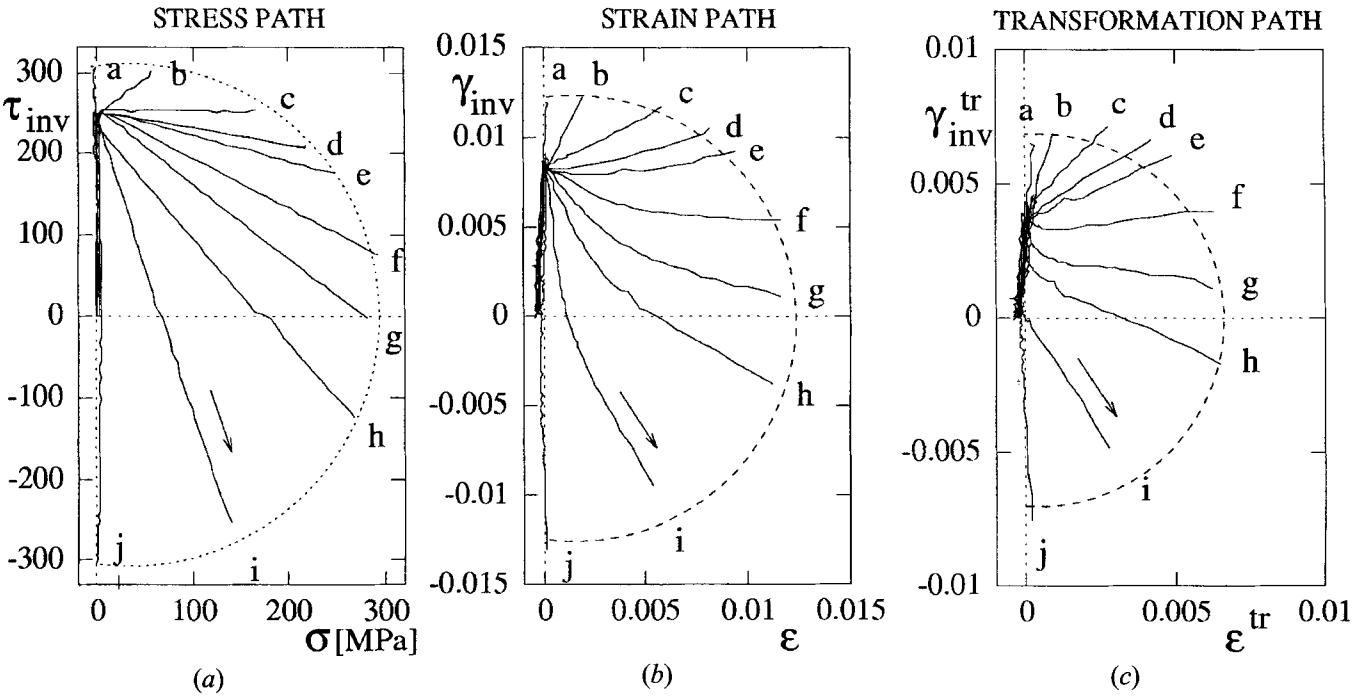

Fig. 13—The strain response of partially transformed SMA polycrystal to the change of stress paths along directions a through j; stress control, T = 285 K; maximum equivalent stress σ_{eq}^{M} = 300 MPa: (*a*) imposed stress paths, (*b*) strain paths, and (*c*) transformation paths

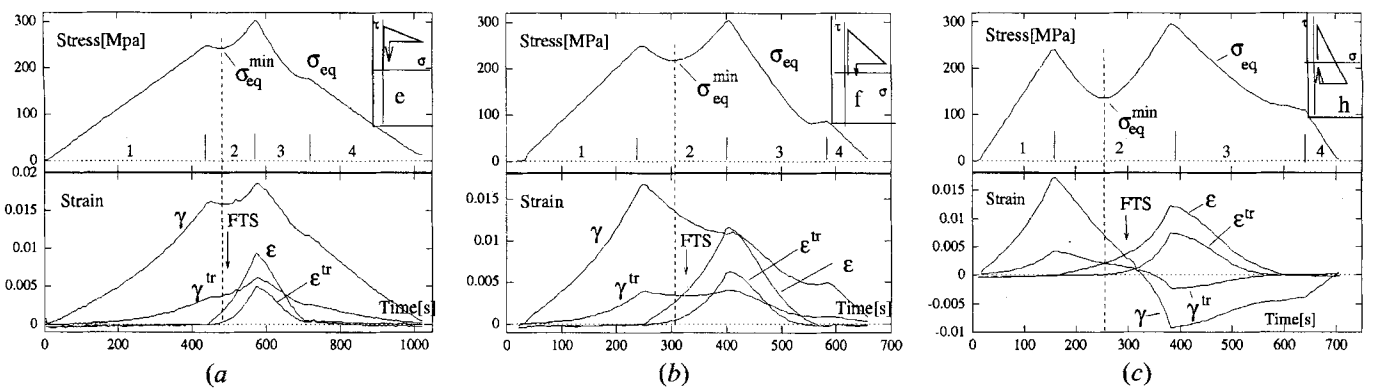

Fig. 14—The development of total and transformation strains in time records of three nonproportional tests from Fig. 13: (*a*) stress path e, (*b*) stress path f, and (*c*) stress path h; FTS marks the stage of the test when the forward transformation starts again during reloading of the stress-induced martensite.

place or does the reverse transformation stop uncompleted, while new martensite variant particles nucleate and grow, causing thus the decrease of torsion+ transformation strain component, γ_{inv}^{tr}? How the MT proceeds on the microlevel of transforming martensite variant particles at such general stress conditions remains a theme for further experimental and theoretical investigations.

IV. CONCLUSIONS

The following basic characteristics of the general stress-induced transformation pseudoelasticity have been found in combined tension-torsion experiments with thin tubular Cu-Al-Zn-Mn SMA polycrystalline specimens.

1. The thermoelastic MT was induced by external stress varying in a general nonproportional way during the pseudoelastic cycle. Transformation paths of SMA polycrystal (the evolution of average transformation strain) were systematically studied and are presented.
2. The progress of the general stress-induced thermoelastic MT in SMA polycrystal can be considered as triggered and controlled by the supplied mechanical work (a kind of equivalent stress).
3. Regardless of the shape of the simple strain (stress) path imposed, the pseudoelastic strains in a simple loading-unloading nonproportional mechanical cycle are completely reversible, provided that the axial loading-unloading strain of comparable magnitude is reversible.
4. The axial strain can be controlled by the change of torque and *vice versa* due to the coupling among tension and torsion under stress, not only in forward transformation, but also in reverse transformation on unloading.
5. Pseudoelastic strains induced by general combination of

external forces are path dependent but very well reproducible along the same stress path.

ACKNOWLEDGMENTS

The support by grants from the Japanese Ministry of Education and Iketani Science Foundation is greatly acknowledged.

REFERENCES

1. K. Otsuka and K. Shimizu: *Int. Met. Rev.*, 1986, vol. 31, pp. 93-114.
2. P. Wollants, J.R. Roos, and L. Deleay: *Prog. Mater. Sci.*, 1993, vol. 37, pp. 227-88.
3. M. Kato and H. Pak: *Phys. Status Solidi B*, 1984, vol. 123, pp. 415-24.
4. Ping Xu and J.W. Morris: *Metall. Trans. A*, 1993, vol. 24A, pp. 1281-94.
5. K. Tanaka, E.R. Oberaigner, and F.D. Fisher: *AMD—Vol. 189 Mechanics of Phase Transformations and Shape Memory Alloys*, ASME, Fairfield, NJ, 1984, vol. 292, pp. 151-57.
6. E. Patoor, A. Eberhardt, and M. Berveiller: *Pitman Res. Notes Math. Ser.*, 1993, vol. 296, pp. 38-54.
7. P. Sittner and M. Tokuda: *Proc. 43rd Natl. Congr. on Theoretical Mechanics*, The Japanese Society of Mechanical Engineers, Tokyo, Japan, 1994, pp. 667-71.
8. T.E. Buchheit and J.A. Wert: *Metall. Mater. Trans. A*, 1994, vol. 25A, pp. 2383-89.
9. E. Patoor, M. El Amrani, A. Eberhardt, and M. Berveiller: *Proc. ESOMAT 94*, 1994, to appear in *J. Phys.*
10. P. Sittner, M. Takakura, and M. Tokuda: *Sc. Metall. Mater,* 1995, vol. 32, pp. 2073-79.
11. P. Sittner and M. Tokuda: *Proc. 15 Risø Int. Symp.—Numerical Prediction of Deformation Processes and The Behavior of Real Materials*, ed. S.I. Andersen, J.B. Bilde-Sorensen, T. Lorentzen, O.B. Pedersen, N.J. Sorensen, Risø National Laboratory, Roskilde, Denmark, 1994, pp. 537-41.
12. P. Sittner, Y. Hara, and M. Tokuda: *Proc. Shape Memory Materials 94*, ed. Chu Youi and Tu Hailing, International Academic Publishers, Beijing, China, 1994, pp. 541-45.
13. P. Sittner, Y. Hara, and M. Tokuda: *Proc. ICSMA-10*, ed. H. Oikawa, K. Maryuama, S. Takeuchi and M. Yamaguchi, The Japan Institute of Metals, Sendai, Japan, 1994, pp. 319-25.